Mineralogical Magazine, December 2012, Vol. 76(8), pp. 3327–3336

Evidence for gas-induced pathways in clay using a nanoparticle injection technique

J. F. Harrington*, A. E. Milodowski, C. C. Graham, J. C. Rushton and R. J. Cuss

British Geological Survey, Keyworth, Nottingham NG12 5GG, UK

[*Received 19 December 2011; Accepted 03 October 2012; Associate Editor: Nicholas Evans*]

ABSTRACT

Corrosion, water radiolysis and microbial degradation will result in the generation of gas within repositories designed for the geological disposal of high-level radioactive waste. It is therefore crucial in the design of such facilities that the relevant mechanisms allowing gas migration through repository materials, both engineered barriers and clay-based candidate host rocks, are correctly identified. In Belgium, the Boom Clay represents a candidate host material for which the advective gas breakthrough characteristics and transport properties have been extensively tested and are well defined by numerous studies. The Boom Clay displays a significant capacity for self-sealing and both laboratory and field tests indicate that advective gas transport occurs not by visco-capillary flow, but instead through the formation of pressure-induced dilatant pathways. In this study, we present results from a gas injection test designed to demonstrate the presence of these features by injecting nanoparticulate tracers with helium gas into a sample of Boom Clay. The results provide conclusive evidence for the formation of transient, dilatant gas pathways within a candidate clay-based host rock. This technique provides a novel diagnostic tool for the identification of processes governing multi-phase flow, supporting robust long-term assessments of repository performance.

Keywords: Boom Clay, gas flow, geological disposal, nanoparticles, radioactive waste.

Introduction

A full understanding of the migration behaviour of gas generated during canister corrosion is of fundamental importance to the development of geological disposal facilities for radioactive waste. There is significant evidence that in some scenarios the rate of gas production may exceed the diffusional capacity of the engineered barriers and clay-based candidate host rocks (Weetjens and Sillen, 2006; Ortiz *et al*., 2002; Wikramaratna *et al*., 1993). If this occurs, capillary restrictions (Aziz and Settari, 1979) on the movement of gas will result in the build-up of pressure to a critical value. To accurately predict the movement of gas through argillaceous materials (Neretnieks, 1984; Kreis, 1991; Askarieh *et al*., 2000; Ekeroth *et al*., 2006; Smart *et al*., 2006), it is first necessary to define the correct conceptual model that best represents the empirical data. Four such models for gas flow exist: (1) gas movement by solution and/or diffusion governed by Henry's and Fick's laws, respectively; (2) gas migration by visco-capillary flow, governed by a generalized form of Darcy's Law; (3) gas flow through dilatant pathways, the permeability of which is dependent on an interplay between local gas pressure and the effective stress state; and (4) gas flow along macro fractures similar in form to those observed in hydrofracture activities during reservoir stimulation, where fracture initiation occurs when the gas pressure exceeds the sum of the minor principle stress and tensile strength. For engineering problems such as radioactive waste disposal, underground gas storage and carbon dioxide sequestration, most interest is focussed on

* E-mail: jfha@bgs.ac.uk
DOI: 10.1180/minmag.2012.076.8.45

understanding the processes and mechanisms governing the advective transport of gas (mechanisms 2–4).

Past laboratory and field tests indicate that, in the case of the Boom Clay, advective gas flow occurs through the creation of transient, localized pathways, rather than standard visco-capillary flow (Horseman and Harrington, 1994; Ortiz *et al*., 1996, 2002; Harrington and Horseman, 1997, 1999). These pathways have been shown to form in a number of argillaceous materials and are pressure-induced features (Horseman and Harrington, 1994, 1999; Gallé and Tanai, 1998; Horseman *et al*., 1999; Ortiz *et al*., 2002; Autio *et al*., 2006; Angeli, 2009), the aperture of which is a function of the internal gas pressure and structural constraints within the clay. However, the presence and spatial distribution of such features has not yet been directly imaged.

The purpose of this study is not to define the (already well characterized) breakthrough properties of Boom Clay, but to provide the first direct microscale evidence for this mechanism of flow. To help differentiate between competing theories and processes, a novel technique has been developed utilizing the injection of nanoparticles in a gaseous stream, to provide new insight into the formation, geometry and distribution of conductive pathways. In the results section we present images showing localized aggregates of gold and hydrophobic titanium oxide (TiO_2) nanoparticles, successfully injected into the clay, and draping of the host fabric around nanoparticle aggregates; clearly demonstrating the principle of plastic self-sealing which is commonly attributed to such materials. This method and the resulting observations represent a completely new approach to imaging ephemeral fluid flow pathways, which will aid investigations into the scale and nature of gas migration through low-permeability clays and mudrocks. Such observations are of direct relevance to a broad range of geoscientific problems, from the disposal of heat-emitting radioactive waste to the geological storage of carbon dioxide.

Methodology

A well-preserved sample of Boom Clay, deposited in the north European sedimentary province during the middle Oligocene, (Tertiary period, ~30 Ma) was taken from drilling CG R13U in the HADES underground research laboratory (located at Mol, in northeast Belgium) at a depth of 178.6 m TAW[1]. This was sub-sampled (to minimize perturbation) and a number of cylindrical specimens (50 mm diameter × 25 mm length) were manufactured using standard geotechnical techniques for poorly consolidated clays (dry-cutting with a stainless steel ring-former with a sharp, leading edge). Gallé and Tanai (1998) demonstrated that gas entry pressure is dependent upon the initial saturation of the clay. Prior to testing the sample saturation was estimated (assuming a grain density of 2680 kg m^{-3}) to be ~93.1%. However, given the plasticity of Boom Clay and its capacity for self-sealing (Davies, 2005), the application of confining pressure is likely to affect the effective saturation under test conditions. Assuming ideal gas behaviour, the degree of saturation of a compressible clay-like material under confinement, S_r^{tc}, can be estimated as a function of the void ratio and saturation at atmospheric conditions, e^{at} and S_w^{at}, respectively, as follows (Horseman and Harrington, 1997):

$$S_r^{tc} = \frac{wG_s}{e^{at}(S_w^{at}) + e^{at}(1 - S_w^{at})R_p}$$

where R_p is the ratio of atmospheric pressure to the air pressure in the sample when subjected to confinement, w is the gravimetric water content and G_s is the average specific gravity of the mineral solids. Under the conditions applied in this experiment, and assuming that as much as 80% of the confining pressure is carried through the sample fabric rather than the pores, this leads to an estimated effective saturation of 99%, even before allowing for any additional dissolution of gas into solution. As such, it seems unlikely that a fully interconnected pathway of gas was present within the sample prior to gas injection. This assertion is borne out by observations presented in the results section of this paper. It should be noted that, due to the introduction of additional mass (injected particles) into the sample (and remaining at the sample interface), it was not possible to derive the post-test saturation of the sample.

A 50:50 mixture (by volume) of gold and hydrophobic coated TiO_2 nanoparticles (MK Impex, Canada: at <100 nm and <50 nm, respectively) was selected as a tracer for the gas injection experiment. Gold nanoparticles were

[1] TAW stands for Tweede Algemene Waterpassing which is the Belgian national datum.

https://doi.org/10.1180/minmag.2012.076.8.45 Published online by Cambridge University Press

chosen for their very high backscattered electron coefficient (due to density and large atomic number) and natural absence within the Boom Clay. As such, the gold can be readily differentiated by scanning electron microscopy (SEM) techniques, even in nanoparticle form. In the initial development of this technique, gold nanoparticles alone were used as a tracer, but their tendency to aggregate, led to poor dispersion in the clay. In the experiment presented here, mixing of the gold nanoparticles with additional TiO_2 nanoparticles (50:50 by volume) allowed aggregation to be reduced and dispersion improved.

The test sample was sandwiched between two stainless-steel platens, with the nanoparticle mixture preloaded into a recess located within the injection platen. The sample was isolated from the confining fluid (deionized water) using a flexible Teflon sheath and an isotropic confinement of 2.2 MPa was applied to the clay. Injection and confining pressures were controlled using two high-precision ISCO syringe pumps (following the technique outlined by Harrington *et al*., 2009). As gas could potentially leak past the syringe seal, the injection pump was charged with water which was used to displace helium into the sample from a pre-charged vessel. This approach also ensures that the helium is water-saturated in advance, negating the possibility that it may desiccate the clay.

The mass flux of gas per unit time, t, into the clay during gas injection testing was derived using a data reduction algorithm based on the ideal gas law. At any point in time, the total volume of the injection system V_s is:

$$V_s = V_w + V_g$$

where V_w and V_g are the volume of water and gas respectively. As the injection pump advances (i.e. water is injected into the interface vessel), the volume of gas reduces by an equal amount as compression of the gas occurs:

$$(V_g)_{(t)} = V_s - (V_w)_{(t)}$$

By applying the ideal gas law, where P is the gas pressure, n is the number of moles of gas in the system, R is the universal gas constant and T is ambient temperature, the number of moles of gas injected into the clay is:

$$n_{t=0} - n_t = \frac{P_{t=0}(V_g)_{t=0} - P_t(V_g)_t}{RT}$$

Hence, by multiplying the ideal gas law by the molar volume of gas (taken as $0.02241 m^3\ mol^{-1}$) defined at standard temperature and pressure conditions (STP[2]), the equivalent volumetric flow rate of gas (at STP) injected into the clay can be obtained.

At day zero, helium injection was initiated through one platen, at a constant rate of $1650\ \mu l\ hr^{-1}$, and the opposing filter was maintained at atmospheric pressure. This generated an increasing differential pressure across the sample with time (Fig. 1), whilst the resulting gas inflow was continuously monitored (Fig. 2). This phase of gas testing continued for just over six days, during the course of which no clear evidence for gas breakthrough was observed. Once the applied gas pressure reached a value of 2.37 MPa, the upstream pressure was reduced to 2.1 MPa and the injection pump was switched to maintain this at a constant value. As such, the test history is non-ideal, in that the applied gas pressure was allowed to briefly exceed the confining pressure (for a period of 3 hours) by a maximum value of 0.27 MPa. However, any impact on sample behaviour is unlikely for a number of reasons: (1) a simple force balance analysis demonstrates that the force applied through the area of the injection filter during this time is negligible in comparison to the force applied to the sample by the confining pressure transferred by the injection platen; (2) the sample sheath was locked into position, providing some additional resistance to tensile strain; (3) there was no evidence for inflow into the sample at this time (or for the following three days), as might be expected if the sample was no longer gas-tight.

Following this event, constant gas pressure was maintained for an additional three and a half days, at which time (day 9.3) a notable increase in inflow was detected, indicating gas entry into the specimen. This inflow continued until day twelve when the pump ran out of fluid and the test was terminated. Such 'time-dependent' breakthrough behaviour has previously been observed in other argillaceous materials (Harrington *et al*., 2012) and it has been suggested that this 'delay' is related to the requirement for the generation of a sufficient network of dilatant pathways prior to significant gas migration.

[2] Defined as 273.15 K and 101.325 kPa.

https://doi.org/10.1180/minmag.2012.076.8.45 Published online by Cambridge University Press

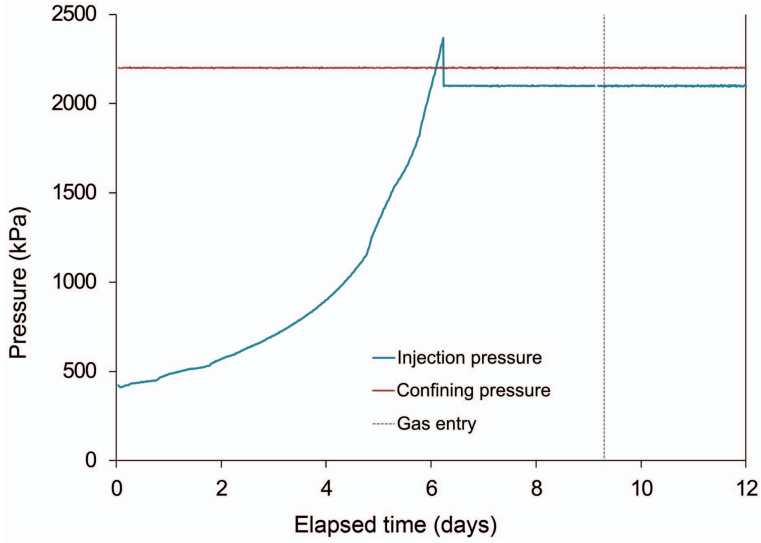

FIG. 1. Evolving upstream (injection) pressure and applied confining pressure during gas injection testing. Gas was pumped at a constant flow rate from days 0–6, leading to a rapid increasing in the applied gas pressure, with no clear evidence of gas entry into the sample. Due to proximity to the confining pressure, the upstream was then reduced to 2.1 MPa and maintained at a constant value until the end of the test (day 12).

Upon test completion, the core was examined using a combination of optical and electron microscopy for evidence of gold and TiO_2 nanoparticle penetration. This was facilitated by submerging the sample in liquid nitrogen, thereby embrittling the clay. It was then split

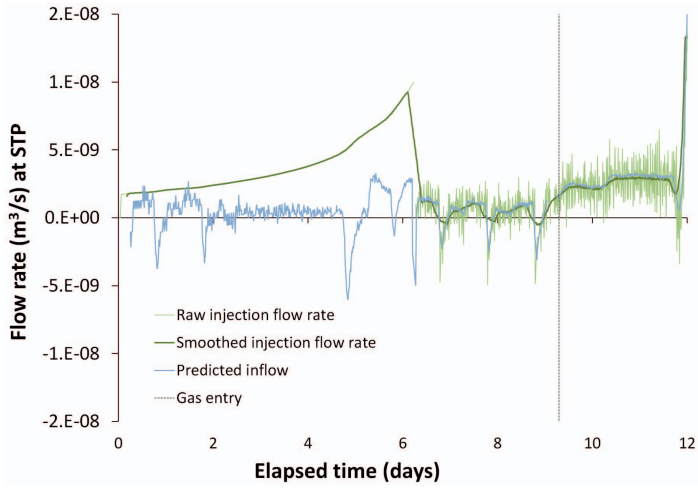

FIG. 2. Evolving upstream (injection) flow rate and associated inflow. Injection was at a constant flow rate of 1650 μl hr^{-1} leading to a growing applied gas pressure. (This is the cause of the increasing flow rate observed when converted to standard temperature and pressure). Changes in flow rate after day 7 represent those required to maintain a constant gas pressure of 2.1 MPa. The marked daily oscillations in flow rate observed during the test are the result of temperature fluctuations in the laboratory. A clear elevation in injection flow rate is observed at day 9.3, which is also apparent as a notable increase in inflow. This marked change in behaviour is the first clear evidence for gas entry into the Boom Clay sample.

https://doi.org/10.1180/minmag.2012.076.8.45 Published online by Cambridge University Press

axially (on its side to prevent contamination), providing a longitudinal profile through the core, perpendicular to the gas injection point. The freshly fractured surfaces were photographed and visually examined under a binocular optical microscope. Higher resolution observations were then undertaken using a FEI QUANTA 600 environmental scanning electron microscope (ESEM) equipped with an Oxford Instruments INCA Energy 450 energy-dispersive X-ray microanalysis (EDXA) system with a 50 mm^2 X-Max silicon-drift detector. The fracture surfaces were examined directly in the ESEM under low vacuum (0.98 Torr H_2O), without a conductive coating in both secondary (SE) and backscattered electron imaging (BSE) modes, using a 10 kV beam. The EDXA was used to aid nanoparticle identification and to map the distribution of gold and TiO_2 particles on the fractured clay surface.

Experimental observations

Flow observations and post-test sample imaging indicate that a network of conductive gas pathways was successfully established across the specimen during testing. Flux across the sample was maintained for sufficient time to promote the ingress of nanoparticles. Upon completion of the injection stage the sample was removed from the apparatus. Visual and optical microscope observations showed that the freshly-fractured core surface displayed a very diffuse, pale bluish white 'bloom', extending from immediately beneath the nanoparticle injection cake to a distance of up to 20 mm into the sample, as a 'tongue-like' plume with a generally narrowing tail running approximately parallel to the core axis (Fig. 3*a*). Small diffuse lobes were also observed to spread laterally from the margins of the main plume, parallel to the bedding lamination (the core axis was perpendicular to bedding

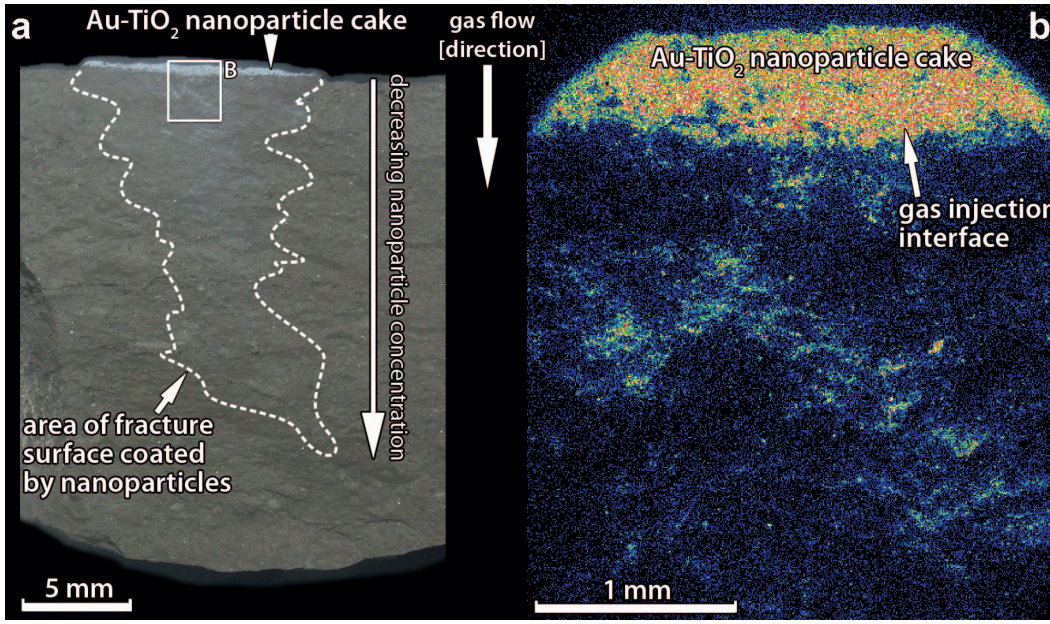

FIG. 3. (*a*) Photograph of one surface of the longitudinally-fractured clay core displaying a tongue-like area with a bluish white discolouration or 'bloom' (due to coating by a fine film of TiO_2 nanoparticles) penetrating into the core from immediately beneath the gold-TiO_2 nanoparticle cake at the point of gas injection. Although rapid freezing in liquid nitrogen will open planes of weakness, the nanoparticles were injected prior to freezing and therefore identifying a plane of weakness which was present prior to freezing. (*b*) An EDXA elemental map for Ti distribution recorded from a part of the fractured core surface close to the gas injection interface, displaying the discolouration plume in Fig. 3. The map shows that the discoloration plume corresponds to the concentration of TiO_2 nanoparticles that penetrated into the core during gas injection.

https://doi.org/10.1180/minmag.2012.076.8.45 Published online by Cambridge University Press

lamination). Elemental mapping showed that the plume of bluish white discolouration observed on the fractured core surface corresponded precisely with areas of high TiO_2 concentration (Fig. 3*b*). High-resolution SEM observations showed that the fractured clay surface in these areas was coated with a very fine, diffuse film of TiO_2 nanoparticles combined with large 'fluffy' aggregates of TiO_2 nanoparticles (Fig. 4*a*). The EDXA elemental mapping also showed that the TiO_2 nanoparticle-aggregates were concentrated along a series of small, interconnected, sub-horizontal, braided, 'step-like' features or channels in the broken core surface. These correspond to where the core has broken along a network of very fine, anastomosing sub-vertical, laterally discontinuous microfractures (orientated sub-parallel to the core axis) and their intersection with the bedding lamination.

In contrast to the TiO_2 nanoparticles, elemental mapping showed that gold nanoparticles were only very sparsely distributed (and barely detectable) on the fractured core surface, except within the nanoparticle cake and where relatively large aggregates of gold nanoparticles had penetrated into sandy laminae just beneath the point of gas injection. Although improved dispersion of the gold nanoparticles was achieved through using a mixture of gold and TiO_2 nanoparticles, the analyses revealed that the gold nanoparticles still clumped together in much coarser aggregates than the TiO_2 nanoparticles. The gold nanoparticle aggregates were usually seen to be enclosed within a mass of finer TiO_2 nanoparticles on the fractured clay surface. However, nanoparticle aggregates and isolated nanoparticles of gold were also seen to be trapped and enclosed within the clay matrix of the rock (Fig. 4*b*). The gold nanoparticle aggregates typically varied between <0.5 and 4 μm in diameter, but close to the gas injection interface reached up to 10 μm in size. The aggregate

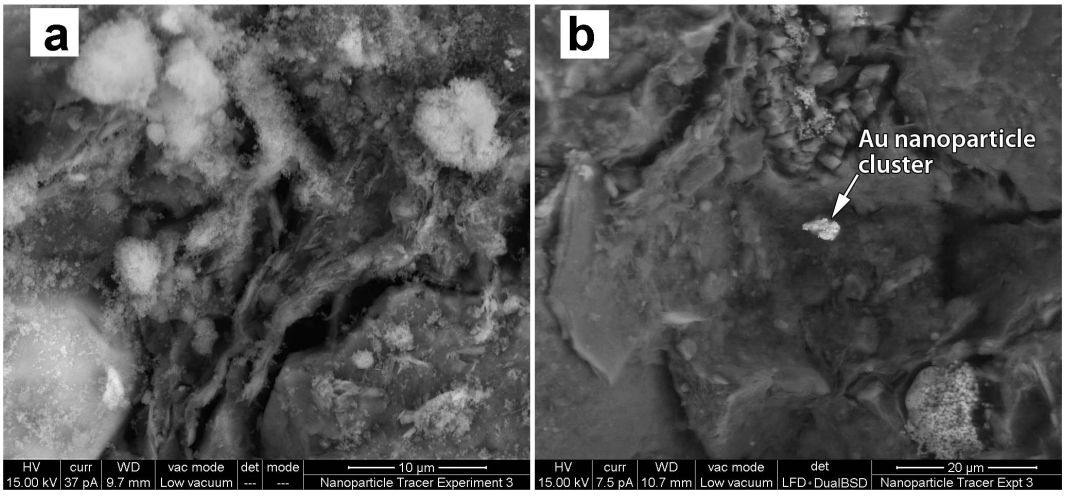

FIG. 4. (*a*) A combined SE and BSE image showing finely dispersed and 'fluffy' aggregates of TiO_2 nanoparticles (white) coating the fractured clay surface. Although authigenic anatase is present within the Boom Clay as a diagenetic alteration product of unstable ferromagnesian minerals, ilmenite or titanian magnetite, it can be differentiated from the TiO_2 within the nano powder for the following reasons: the TiO_2 within the nanoparticle plume is far too abundant, covering a large proportion of the fracture surface in comparison to the natural TiO_2, which is only present in trace amounts; the trail of TiO_2 nanoparticles clearly originates from the point of injection (Fig. 3), and is not uniformly distributed across the sample, or concentrated in heavy mineral bands, as would be expected for naturally occurring anatase; mapping clearly shows little or no detectable TiO_2 in the Boom Clay in fractured areas outside the plume due to its low level of concentration; whereas gold nanoparticles are not as well dispersed across the fracture surface, there are sufficient gold particles present in association with the mapped TiO_2 to be confident that it stems from the nanoparticle assemblage injected into the sample. (*b*) Mixed SE and BSE image showing an aggregate of gold nanoparticles embedded within the clay matrix from a site 17 mm from the injection face. Figure 3 shows the distribution of gold and TiO_2 along the fracture plane which was exposed following immersion of the sample in liquid nitrogen and splitting of the core.

https://doi.org/10.1180/minmag.2012.076.8.45 Published online by Cambridge University Press

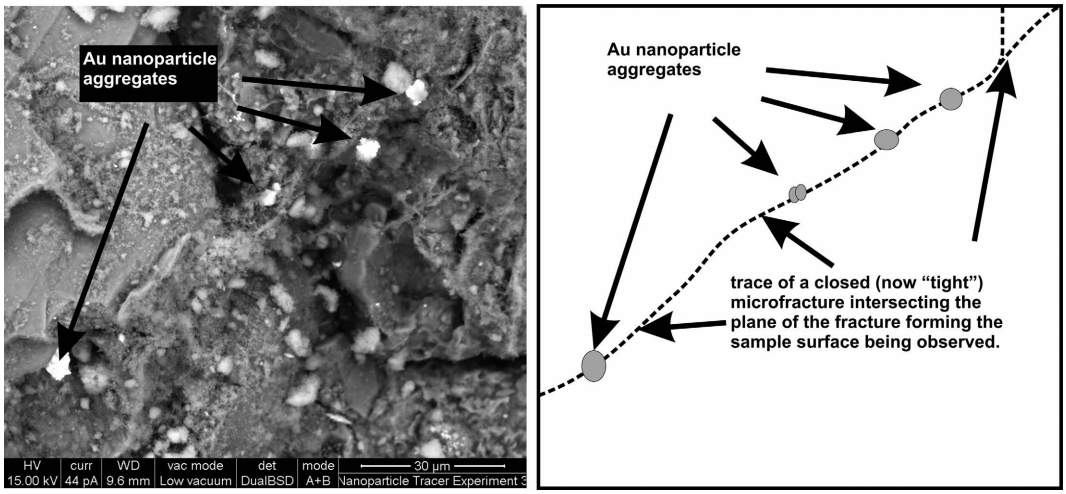

FIG. 5. A combined SE and BSE image showing a trail of aggregated gold nanoparticles trapped within the trace of a now closed pathway. The Au particles are trapped along what appears to be a healed pathway that is sub-orthogonal to the plane of the fracture surface imaged in Fig 3*a*,*b*. The pathway in Fig. 5 appears to have collapsed, encasing the gold particles after they were injected. The gold particle aggregates are clearly much larger in diameter than the width of the pathway trace, providing conclusive evidence for the existence of dilatant pathways. These features must be at least equal in aperture to the size of the gold aggregates otherwise penetration of the clay would not have occurred.

diameter generally decreased with increasing distance from the gas injection interface, but traces of the gold nanoparticles could be found up to 20 mm from the point of gas injection.

Linear 'trails' (up to 300 µm long) of gold and TiO_2 nanoparticles were observed trapped within the clay matrix in the fractured clay surface (Figs 5 and 6). These appear to delineate the probable traces of sealed pathways intersecting with the freshly broken core surface being observed under the ESEM. Larger open microfractures were also observed, usually developed parallel to bedding. These are quite different to the healed microfractures, and were largely devoid of gold and TiO_2 nanoparticles (Fig. 6), and attributed to post-experimental artefacts produced by sample shrinkage during drying in the ESEM instrument. Similar nanoparticle aggregates were rarely seen to be present along the grain boundaries of quartz and feldspar silt particles (Fig. 7). These observations indicate that the nanoparticles have been injected along transient pathways, through the clay matrix and around grain boundaries of coarser detrital siliciclastic silt and sand grains, which were induced and dilated during gas injection. It would appear that these features then sealed, trapping any nanoparticles that were being transported in the gas stream. The size of the nanoparticle aggregates, typically between 0.5 and 4 µm (though up to 10 µm diameter), provides an indication of the minimum aperture of the dilatant pathways induced in the clay during gas injection.

Conclusion

This study has successfully demonstrated that gold and TiO_2 nanoparticles can be introduced into a gas stream and used as a tracer for studying gas transport pathways through clay or mudrock. This is the first time that the location of gas pathways within low permeability mudrock or clays have been directly observed, and provides a new insight into the mechanism of gas migration through these rocks. These observations highlight the potential importance of dilatancy as a fundamental process in the advective movement of gas through such materials. These observations support previous indirect measurements which indicated the existence of such features (Horseman and Harrington, 1994; Ortiz *et al*., 1997, 2002; Rodwell, 2000; Harrington and Horseman, 1999; Van Geet *et al*., 2008; Angeli *et al*., 2009). The SEM observations show that relatively large aggregates of gold nanoparticles,

https://doi.org/10.1180/minmag.2012.076.8.45 Published online by Cambridge University Press

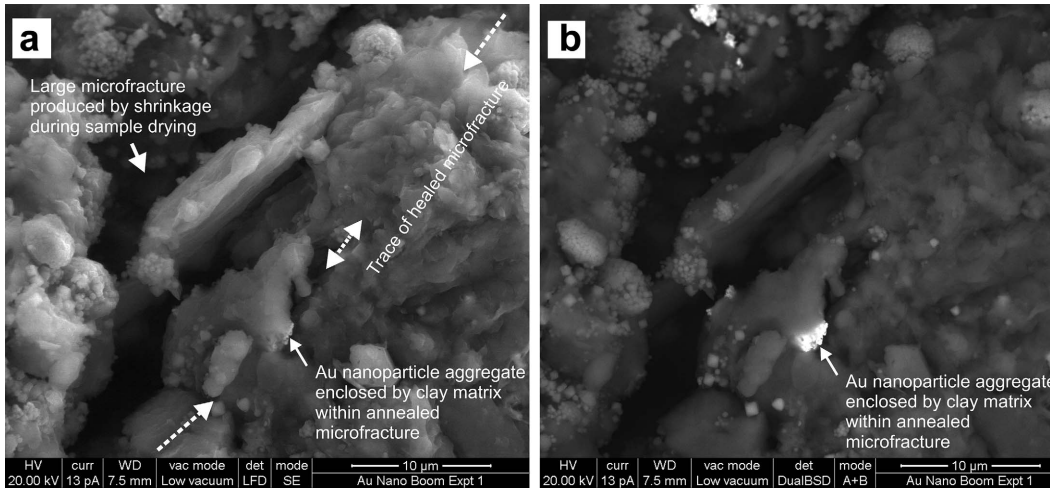

FIG. 6. (*a*) A SE image and (*b*) corresponding BSE image of the same area. A hairline trace of a healed microfracture (arrowed) is just discernible in the SE image (*a*) but cannot be readily recognized in the BSE image (*b*). However, a large aggregate of gold nanoparticles (bright) is seen in the BSE image (*b*), which lies within the trace of the healed microfracture seen in the SE image (*a*) and can be seen to be completely enclosed by clay which drapes around the gold aggregate within the now-collapsed microfracture. Larger dilated microfractures seen parallel to the orientated clay fabric are devoid of gold and titanium nanoparticles and are post-experimental artefacts produced by sample drying and shrinkage in the ESEM instrument.

generally between 0.5 to 4 µm in diameter, and up to 10 µm, have been injected with the gas stream,

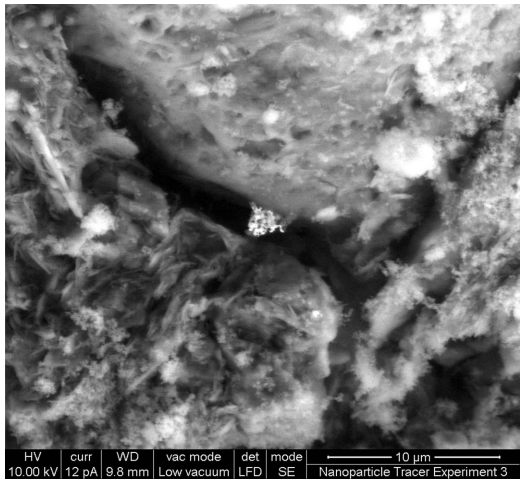

FIG. 7. Mixed SE image showing an aggregate of gold nanoparticles (bright, centre) trapped within a grain boundary microfracture around a quartz silt particle. The microfracture aperture is exaggerated by shrinkage of the clay due to drying under vacuum during SEM observation.

migrating through pressure induced pathways for distances up to 20 mm from the point of injection. This continuous network of pathways is approximately two orders of magnitude larger than the average pathways dimensions for undisturbed clay based on mercury intrusion porosimetry (Dehandschutter *et al*., 2004). The size distribution of aggregates entrained within the clay matrix clearly indicates variable pathway apertures. Current understanding of such features is that they collapse as gas pressure decays to a critical threshold (Horseman and Harrington, 1994; Ortiz *et al*., 1996; Harrington and Horseman, 1999, 2003; Rodwell, 2000). Gold (and TiO_2) nanoparticles are trapped within the clay matrix, forming inclusion trails. These 'strands' of particulates delineate the traces of formerly conductive pathways, which have then collapsed, providing conclusive evidence of pathway closure. These pathways appear to be ephemeral features opening and closing with the passage of gas. The capacity to differentiate process (i.e. viscocapillary flow *vs*. pathway dilation) is fundamental when attempting to accurately describe the multi-phase flow behaviour of argillaceous media, particularly when predicting the long-term behaviour of such materials used

https://doi.org/10.1180/minmag.2012.076.8.45 Published online by Cambridge University Press

for the disposal of heat emitting radioactive waste or as caprocks for the disposal of CO_2.

Acknowledgements

Studies on nanoparticle migration were funded as a component of the BGS Geosphere Containment and Development of Capability projects (part of NERC's National Capability Programme). This work is dedicated to Dr Steve Horseman, who pioneered research on the movement of gas through clay-based host rocks and engineered barriers. He sadly died before nanoparticle injection was available as a viable method for the direct imagining of dilatant pathways, which supports his long-held belief for the importance of such features in multi-phase flow in clay-rich materials. In addition, the authors wish to thank Norbert Maes and Geert Volckaert (Studiecentrum voor Kernenergie, SCK-CEN) for their long support of this research area and Ondraf Niras for the provision of test material and review comments from both organizations. This paper is published with the permission of the Director, British Geological Survey (NERC).

References

Angeli, M., Soldal, M., Skurtveit, E. and Aker, E. (2009) Experimental percolation of supercritical CO_2 through a caprock. *Energy Procedia*, **1**, 3351–3358.

Askarieh, M.M., Chambers, A.V., Dabniel, F.B.D., Fitzgerald, P.L., Holtom, G.J., Pilkington, N.J. and Rees, J.H. (2000) The chemical and microbial degradation of cellulose in the near field of a repository for radioactive wastes. *Waste Management*, **20**, 93–106.

Autio, J., Gribi, P., Johnson, L. and Marschall, P. (2006) Effect of excavation damage zone on gas migration in a KBS-3H type repository at Olkiluotu. *Physics and Chemistry of the Earth*, **31**, 649–653.

Aziz, K. and Settari, A. (1979) *Petroleum Reservoir Simulation*. Applied Science, London.

Davies, C. (2005) Overview of projects and activities related to EBS processes, carried out as part of the 5th and 6th Euratom framework programmes (1998–2006). Pp 57–65 in: *Engineered Barrier Systems (EBS) in the context of the entire safety case.* Workshop Proceedings, Las Vegas, United States, 14–17 September 2004. OECD, Nuclear Energy Agency No. 6001, OECD Publishing, Paris.

Dehandschutter, B., Vandycke, S., Sintubin, M., Vandenberghe, N., Gaviglio, P., Sizun, J.-P. and Wouters L. (2004) Microfabric of fractured Boom Clay at depth: a case study of brittle–ductile transitional clay behaviour. *Applied Clay Science*, **26**, 389–401.

Ekeroth, E., Roth, O. and Jonsson, M. (2006) The relative impact of radiolysis products in radiation-induced oxidative dissolution of UO_2. *Journal of Nuclear Materials*, **355**, 38–46.

Gallé, C. and Tanai, K. (1998) Evaluation of gas transport properties of backfill materials for waste disposal: H_2 migration experiments in compacted Fo-Ca clay. *Clays and Clay Minerals*, **46**, 498–508.

Harrington, J.F. and Horseman, S.T. (1997) Gas migration in clay. Pp. 153–173 in: *Projects on the effects of gas in underground storage facilities for radioacive waste (Pegasus project). Proceedings of a progress meeting held in Mol, Belgium, 28 and 29 May 1997* (B. Haijtink and W. Rodwell, editors). European Science and Technology Series (1998) EUR 18167 EN.

Harrington, J.F. and Horseman, S.T. (1999) Gas transport properties of clays and mudrocks. Pp. 107–124 in. *Muds and Mudstones: Physical and Fluid Flow Properties* (A.C Aplin, A.J. Fleet and J.H.S. Macquaker, editors). Geological Society of London, Special Publication, **158**. Geological Society of London, London.

Harrington, J.F. and Horseman, S.T. (2003) *Gas migration in KBS-3 buffer bentonite: Sensitivity of test parameters to experimental boundary conditions*. SKB Technical Report TR-03-02.

Harrington, J.F., Noy, D.J., Horseman, S.T., Birchall, J.D. and Chadwick, R.A. (2009) Laboratory study of gas and water flow in the Nordland Shale, Sleipner, North Sea. Pp. 521–543 in: *Carbon Dioxide Sequestration in Geological Media – State of the Science* (M. Grobe, J.C. Pashin and R.L. Dodge, editors). AAPG Studies in Geology, **59**. American Association of Petroleum Geologists, Tulsa, Oklahoma, USA.

Harrington, J.F., de La Vaissière, R., Noy, D.J., Cuss, R.J. and Talandier, J. (2012) Gas flow in Callovo-Oxfordian Clay (COx): results from laboratory and field-scale measurements. *Mineralogical Magazine*, **76**, 3303–3318.

Horseman, S.T. and Harrington, J.F. (1994) *Migration of repository gases in an overconsolidated clay*. British Geological Survey Technical Report WE/94/7. British Geological Survey, Keyworth, UK.

Horseman, S.T. and Harrington, J.F. (1997) *Study of gas migration in Mx80 buffer bentonite*. British Geological Survey, Technical Report WE/97/7. British Geological Survey, Keyworth, UK.

Horseman, S.T., Harrington, J.F. and Sellin, P. (1999) Gas migration in clay barriers. *Engineering Geology*, **54**, 139–149.

Kresis, P. (1991) *Hydrogen evolution from corrosion of iron and steel in low/intermediate level waste*

https://doi.org/10.1180/minmag.2012.076.8.45 Published online by Cambridge University Press

repositories. Nagra Technical Report, NTB 91–21. Nagra, Wettingen, Switzerland.

Neretnieks, I. (1984) Impact of alpha-radiolysis on the release of radionuclides from spent fuel in a geologic repository. *Materials Research Society Symposium*, **26**, 1009–1022.

Ortiz, L., Volcharet, G., De Canniere, P., Aertsens, M., Horseman, S.T., Harrington, J.F., Impey, M., and Einchcomb, S. (1996). *MEGAS – Modelling and Experiments on Gas Migration in Repository Host-rocks*. Nuclear Science and Technology Series, EUR 16746 EN, Luxembourg, 127–147.

Ortiz, L., Volckaert, G. and Mallants, D. (2002) Gas generation and migration in Boom Clay, a potential host rock formation for nuclear waste storage. *Engineering Geology*, **64**, 287–296.

Rodwell, W.R. (editor) (2000) *Research into Gas Generation and Migration in Radioactive Waste Repository Systems (PROGRESS Project)*. Nuclear Science and Technology EUR 19133 EN, European Commission, Luxembourg.

Smart, N.R., Carlson, L., Hunter, F.M.I., Karnland, O., Pritchard, A.M., Rance, A.P. and Werme, L.O. (2006) *Interactions between iron corrosion products and bentonite*. Serco Assurance Report to SKB, SA/EIG/12156/C001.

Van Geet, M., Bastiaens, W. and Ortiz, L. (2008) Self-sealing capacity of argillaceous rocks: review of laboratory results obtained from the SELFRAC project. *Physics and Chemistry of the Earth, Parts A/B/C*, **33**, S396–S406.

Weetjens, E. and Sillen, X. (2006) *Gas Generation and Migration in the Near Field of a Supercontainer-Based Disposal System for Vitrified High-Level Radioactive Waste*. Proceedings of the 11th International High-Level Radioactive Waste Management Conferance (IHLRWM), Las Vegas, Nevada, USA.

Wikramaratna, R.S., Goodfield, M., Rodwell, W.R, Nash, P.J. and Agg, P.J. (1993) *A Preliminary Assessment of Gas Migration from the Copper/Steel Canister*. SKB Technical report TR93–31. Swedish Nuclear Fuel and Waste Management Company (SKB), Stockholm, Sweden.

https://doi.org/10.1180/minmag.2012.076.8.45 Published online by Cambridge University Press